Acceleration Harmonics Reduction for Electrodynamic Shaker Fed by Cascaded H-Bridge Inverter

Hung-Chi Chen (IEEE Member)
Department of Electrical and Computer Engineering
National Chiao Tung University
Hsinchu, Taiwan
hcchen@cn.nctu.edu.tw

Jhen-Yu Liao
Department of Electrical and Computer Engineering
National Chiao Tung University
Hsinchu, Taiwan
popoid1003@hotmail.com

***Abstract*—For a permanent magnet electrodynamic shaker (PMEDS), an LC filter is frequently connected in series to filter out the high-frequency voltage to avoid high-frequency harmonic acceleration of the PMEDS table. This paper use a simple current control loop to avoid high-frequency harmonic acceleration instead of an LC filter which may have large size and heavy weight in high-power applications. A cascade H-bridge inverter is used in this paper to lower the output voltage harmonics and current ripple. According to the provided simulated and experimental results, it can be found that the proposed current control can improve the acceleration of the PMEDS.**

I. INTRODUCTION

The vibration test can assay the influence of the vibration to an object and characteristics of a material. In the general product test, the vibration test is a popular test. It is widely used in the circuit boards, electronic components, domestic products, and materials for the research, stress test, reliability test, and analysis of the structure [1].

An equipment of a vibration test contains a permanent magnet electrodynamic shaker (PMEDS), a linear power amplifier, and a monitoring system. The power of the PMEDS is usually provided by an ac power source whose voltage and frequency can be adjusted. The linear power amplifier can provide great vibration performance and has advantage of low distortion [2-3]. But it has disadvantage of heavy weight and huge size and it's efficiency is very low. These drawbacks can be improved by using switching-mode inverter. So the pulse width modulation (PWM) switching mode inverter is widely used for PMEDSs [4-11].

In order to filter the high frequency voltage of the PWM switching mode inverter, an LC filter is used at the output terminal of the inverter [4-13] as shown in Fig. 1. Due to the LC filter, the inverter output voltage v_o is not equal to the armature voltage v_a and the inverter output current i_L is not equal to the armature current i_a.

Therefore, the controller design should take the LC filter into consideration. Complex control, such as Deadbeat control [11-13] and robust control [4-6, 14] are used. The LC filter also has the drawbacks of large size and heavy weight in high power applications. [14] used a direct current control without the LC filter, but the implementation is in analog circuits.

Output voltage harmonics can be reduced by using cascaded H-bridge inverter (CHB) as shown in Fig. 2. Two H-bridge converters are connected in series, and thus, there is five levels in the inverter output voltage v_o.

The earlier controller of a PMEDS has implemented by analog circuits. The digital control is more and more popular in recent years. Digitalization makes the system have the advantages of high reliability, high precision, robustness, programmable, easy to maintain, and easy to modularized design.

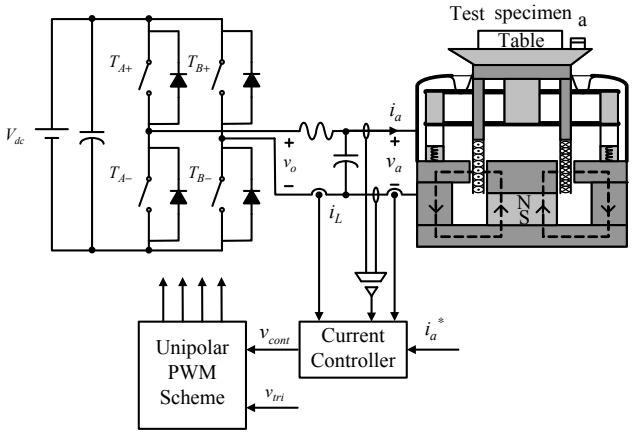

Fig. 1. H-bridge inverter connected with an LC filter [4-6].

This paper uses cascaded H-digital controller which is implemented by an FPGA to control the circuit. The controller uses PWM switching mode to implement the sinusoidal vibration test of the PMEDS for improving the drawbacks of the linear power amplifier. The harmonics of

voltage and current can be reduced by using cascaded H-bridge inverter (CHB) and dead-time compensator instead of an LC filter. Therefore, better current tracking performance and accelerate characteristic can be obtained.

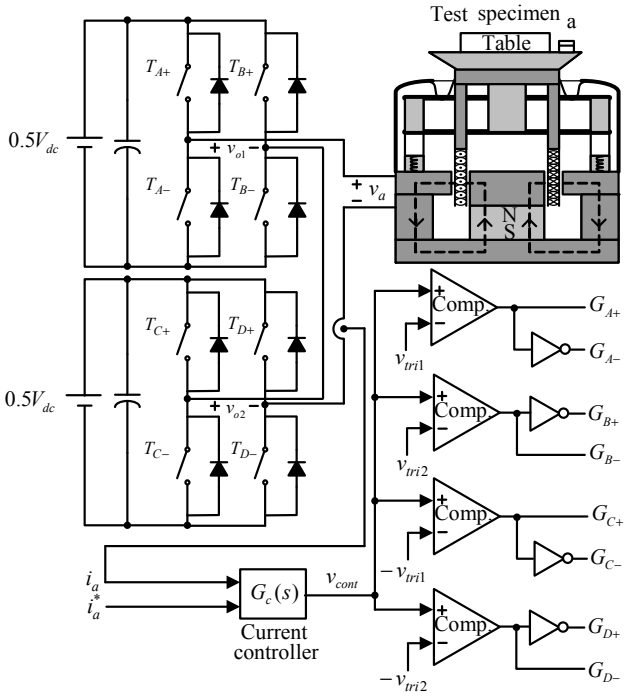

Fig. 2. System configuration plot.

II. PERMANENT MAGNET ELECTRODYNAMIC SHAKER

In order to simplifier the analysis, here are some assumptions:

(1)The PMEDS is a two degrees of freedom (2DOF) mechanical system.

(2)The magnetic flux density in the magnet field is a constant.

The PMEDS model consists of a mechanical system and an electrical system. Figure 3 is an electromechanical model of the PMEDS. The two systems are interactive. The mechanical system equals two springs K_S and K_C, two dampers C_S and C_C, and three masses M_S, M_L, and M_C. The K_S and C_S are the PMEDS suspension stiffness and damping coefficient. The K_C and C_C are the stiffness and damping coefficient of the adhesive bounding element which is used to connect the armature coil and the table of the PMEDS. The M_S, M_L, and M_C are the table mass, load mass, and the coil mass. The x_T and x_C are the table and the coil displacements to the PMEDS.

The back electromotive force (EMF) e is proportional to the table velocity v of the PMEDS, and it can be written as

$$e = Bl\frac{dx_C}{dt} = Blv = \Gamma v \tag{1}$$

The electromagnetic force f_{em} produced by the armature current i_a can be written as

$$f_{em} = Bli_a = \Gamma i_a \tag{2}$$

By using the Hooke's law, the force of a spring can be written as

$$f_{sp} = -Kx \tag{3}$$

where K is the stiffness and x is the displacement.

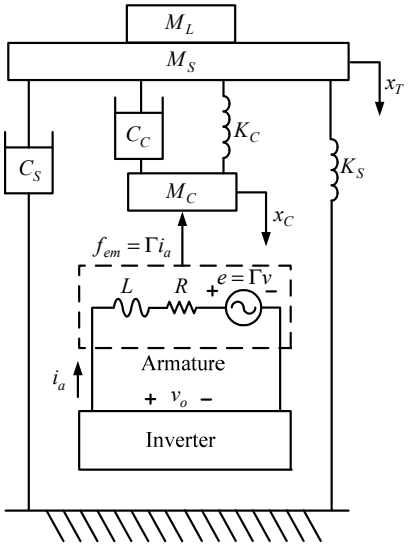

Fig. 3. An electromechanical model of the PMEDS.

The friction force of the object is proportional to the velocity. Therefore the friction force can be written as

$$f_f = -C(dx/dt) \tag{4}$$

where c is the damping coefficient. Use Newton's second laws of motion to combine the force of mechanical system as below.

$$f_{em} = \Gamma i_a = M_C\frac{d^2x_C}{dt^2} + C_C(\frac{dx_C}{dt} - \frac{dx_T}{dt}) + K_C(x_C - x_T) \tag{5}$$

$$\begin{aligned} &C_C(\frac{dx_C}{dt} - \frac{dx_T}{dt}) + K_C(x_C - x_T) \\ &= (M_L + M_S)\frac{d^2x_T}{dt^2} + C_S\frac{dx_T}{dt} + K_S x_T \end{aligned} \tag{6}$$

There are two forces which are applied for the coil mass, table mass and load mass. The transfer function of the table acceleration and armature current can be obtained as below.

$$\begin{aligned} H_{IA} &\overset{\Delta}{=} \frac{a(s)}{i_a(s)} = \frac{x_T(s)s^2}{i_a(s)} \\ &= \frac{\Gamma(C_C s + K_C)s^2}{\left[\begin{array}{l} M_C(M_L + M_S)s^4 + (M_C C_S + C_C M)s^3 \\ +(M_C K_S + C_C C_S + K_C M)s^2 \\ +(C_C K_S + K_C C_S)s + K_C K_S \end{array}\right]} \end{aligned} \tag{7}$$

where $M = M_L + M_S + M_C$. When the vibration frequency is high, the C_S and K_S are zero. The table of PMEDS is only affected by the C_C and K_C. Therefore, the transfer function (7) can be approximated to

$$H_{IAH} \overset{\Delta}{=} \frac{a(s)}{i_a(s)} \approx \frac{\Gamma K_C}{(M_L + M_S)M_C s^2 + MC_C s + MK_C} \quad (8)$$

The 2DOF model is used for high vibration frequency. When the vibration frequency is low, the table mass and the coil mass can be seen as a single mass, and therefore K_C and C_C both are infinite. The transfer function of the table acceleration and armature current can be simplified as below.

$$H_{IAL} \overset{\Delta}{=} \frac{a(s)}{i_a(s)} = \frac{\Gamma s^2}{Ms^2 + C_S s + K_S} \quad (9)$$

The PMEDS has two resonant frequencies. The resonant frequencies of the PMEDS which can be obtained from (8) and (9) are expressed as below.

$$f_{0H} = \frac{\omega_0}{2\pi} = \frac{1}{2\pi}\sqrt{\frac{MK_C}{(M_L + M_S)M_C}} \quad (10)$$

$$f_{0L} = \frac{\omega_0}{2\pi} = \frac{1}{2\pi}\sqrt{\frac{K_S}{M}} \quad (11)$$

f_{0H} and f_{0L} are a higher and lower resonant frequency, respectively. Because the PMEDS used in this paper is the same as [2], the parameters can be found in Table II. From (10) and (11), using the parameters in Table II can obtain that the higher resonant frequency approximately equals 9682Hz(near 10kHz) and the lower one approximately equals 28Hz. Fig. 4 are the bode plots of H_{IA}, H_{IAL} and H_{IAH}.

Table II
PMEDS parameters

$K_S(N/m)$	17557	$M_C(kg)$	0.069
$C_S(N\cdot\sec/m)$	4.36	$M_L(kg)$	0.311
$K_C(N/m)$	224290000	$M_S(kg)$	0.187
$C_C(N\cdot\sec/m)$	43.62	$\Gamma(N/A)$	13.1

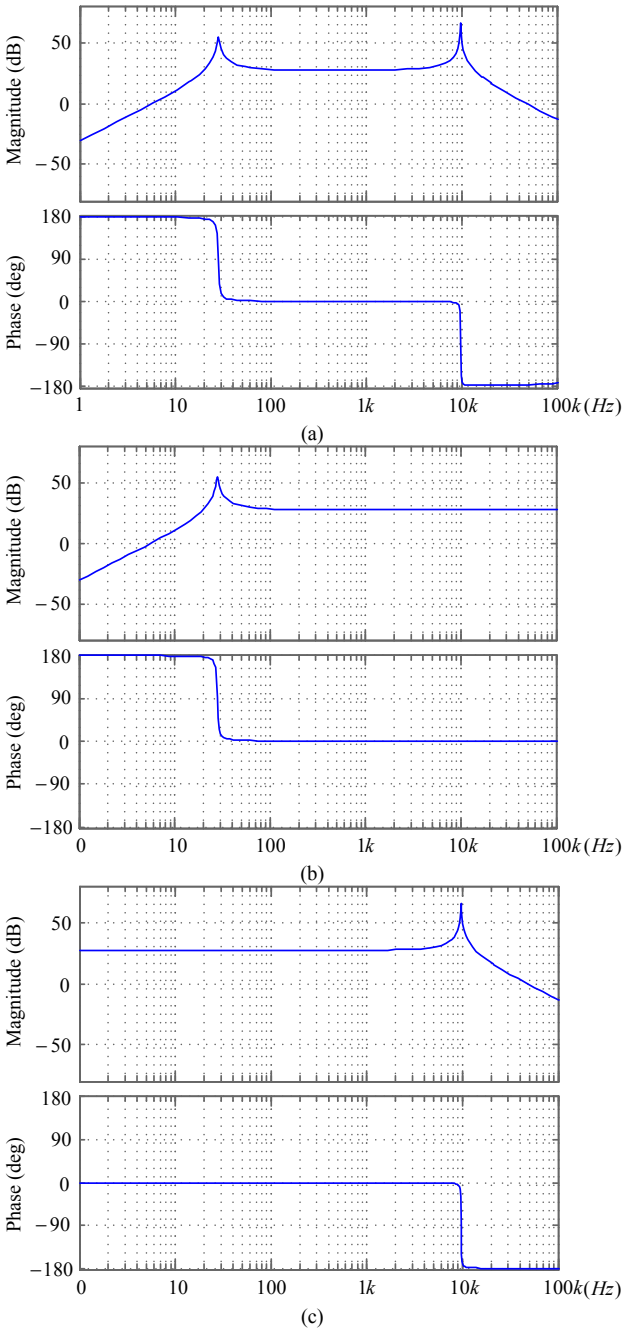

Fig.4. Bode plots of (a) H_{IA}; (b) H_{IAL}; (c) H_{IAH}.

III. CASCADED H-BRIDGE INVERTER

3.1 Harmonic Distribution

In general, unipolar PWM switching scheme is often used in single H-bridge inverter due to its double frequency output voltage characteristics. Figure 5(a) plots the illustrated output voltage waveform of an H-bridge inverter.

Fig. 5(b) shows the illustrated waveform of a cascaded H-bridge inverters. There are 5 levels in the inverter output voltage, and it is noted that the frequency of output voltage ripple in Fig. 5(b) is four times the carrier frequency.

The higher the ripple frequency of output voltage is, the smaller the current ripple is. So the current ripple of CHB is least.

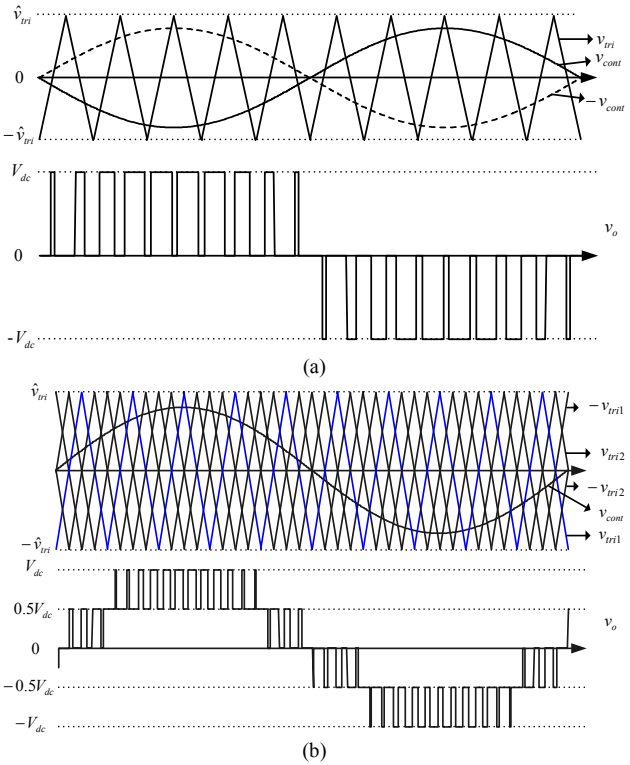

Fig. 5. The waveform of
(a) single H-bridge with unipolar PWM scheme; (b)CHB inverter.

Using Fourier series to expand the output voltage of the inverter, its harmonics is relative to carrier frequency f_{tri} as shown in Fig. 6. From Fig. 6, the harmonics of unipolar H-bridge inverter distribute over sideband of $2f_{tri}$ times. And the harmonics of CHB inverter only distribute over sideband of $4f_{tri}$ times. The magnitude of the harmonics of the CHB is smaller than the others.

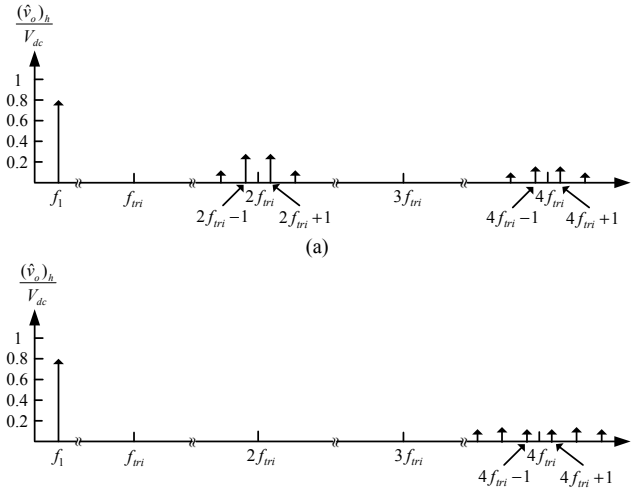

Fig. 6. The harmonics spectrum of
(a) single H-bridge with unipolar PWM scheme; (b)CHB.

3.2 Effect of Dead-Time

In order to prevent short circuit in the H-bridge inverter, it usually adds dead-time to the gate signal. In this paper, dead-time t_Δ also adds to the CHB. But dead-time would influences the output voltage as shown in Fig. 7 shows. Dead-time may increase or decrease the output voltage which depends on direction of the output current. The current in Fig. 7 is positive, and the output voltage in Fig. 7 decreases because of the dead-time. On the contrary, when the current is negative, the output voltage increases. The output voltage of CHB can be expressed as

$$v_a = \left[\frac{v_{cont}^{'}}{\hat{v}_{tri}} - 2\frac{t_\Delta}{T_s} * sign(i_a) \right] V_{dc} \tag{12}$$

where

$$sign(x) = \begin{cases} 1, x > 0 \\ -1, x < 0 \end{cases} \tag{13}$$

The last term of (12) is the influence of the dead-time, and it should not appear in the output voltage.

Duo to the influence of the dead-time, this paper uses a dead-time compensator to eliminate its influence. The magnitude of the compensation is Δv_{cont} . The current controller block diagram which contains a PI controller $G_c(s)$ and a dead-time compensator are shown in Fig. 8. The original command voltage $v_{cont}^{'}$ adds the compensative term Δv_{cont} , and then it equals a new command voltage v_{cont} which enters the CHB.

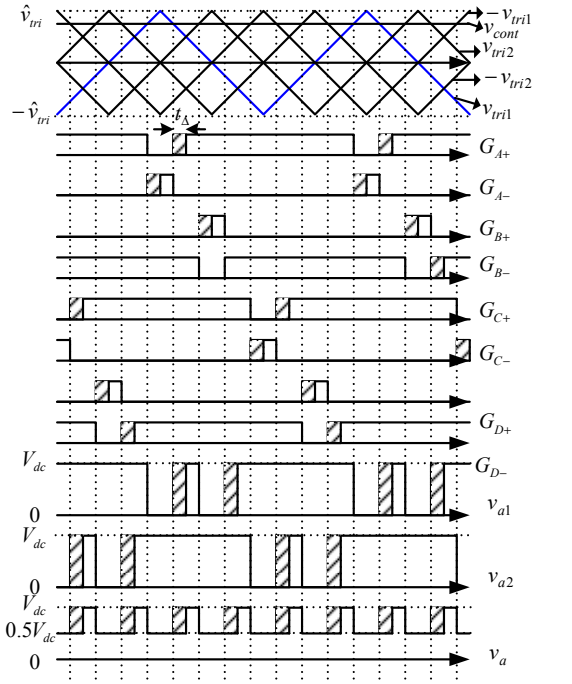

Fig. 7. Dead-time effect of cascade H-bridge converter.

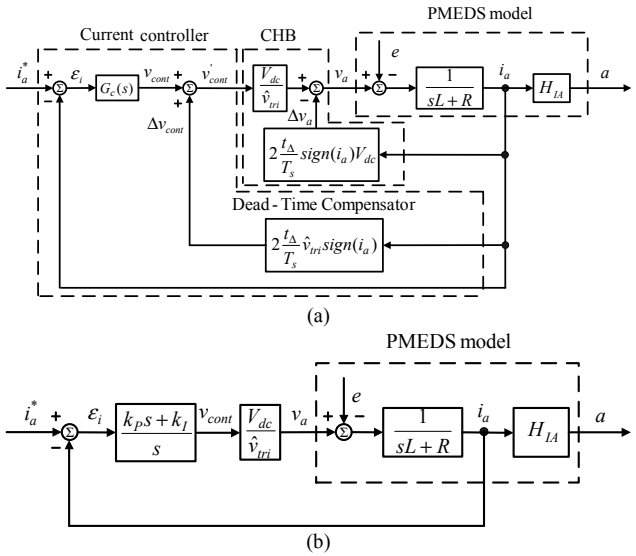

Fig. 8. The control block diagram of the PMEDS.

3.3 Proposed dead-time compensator

The compensative term is

$$\Delta v_{cont} = 2\frac{t_\Delta}{T_s}\hat{v}_{tri} * sign(i_o) \tag{14}$$

The new command voltage is

$$\begin{aligned} v_{cont}' &= v_{cont} + \Delta v_{cont} \\ &= v_{cont} + 2\frac{t_\Delta}{T_s}\hat{v}_{tri} * sign(i_o) \end{aligned} \tag{15}$$

The v_{cont}' in (12) can be replaced by the above equation.

$$v_a = \left[\frac{v_{cont}'}{\hat{v}_{tri}} - 2\frac{t_\Delta}{T_s} * sign(i_a)\right]V_{dc} = \frac{v_{cont}}{\hat{v}_{tri}}V_{dc} \tag{16}$$

The dead-time term is eliminated by the compensative term. The output voltage is proportional to the controller output v_{cont}.

3.4 The design of proportional and integral gain

Fig. 2 is the system configuration plot of this paper. It uses a CHB which provides an output voltage v_a to the PMEDS. It only senses the armature current i_a. The armature current and the armature current command enter the current controller $G_c(s)$. The current controller uses a proportional and integral controller (PI) to produce the control voltage v_{cont}. The current controller $G_c(s)$ can be expressed as

$$G_c(s) = \frac{sk_P + k_I}{s} \tag{17}$$

The control signal v_{cont} compares with two carriers. The phase shift of the each adjacent carrier is $0.25T_s$ where T_s is the PWM switching period.

From Fig. 8(b), in order to simplify the process of designing the proportional and integral gain, the ratio of proportional and integral gain is set to the ratio of inductor and resistor. That is

$$\frac{k_P}{k_I} = \frac{L}{R} \tag{18}$$

Then the transfer function of armature current i_a and armature current command i_a^* can be obtained.

$$\frac{i_a}{i_a^*} = \frac{\frac{k_I k_{PWM}}{R}}{s + \frac{k_I k_{PWM}}{R}} \tag{19}$$

where

$$k_{PWM} = \frac{V_{dc}}{\hat{v}_{tri}} = \frac{1}{10} \tag{20}$$

Equation (19) likes a low pass filter. The pole should be designed in an interval which is between ten times maximum vibration frequency 2kHz of PMEDS and the carrier frequency 50kHz.

$$2\pi\times 2k\times 10 \le \frac{k_I k_{PWM}}{R} \le 2\pi\times 50k \tag{21}$$

When the vibration frequency is 2kHz, the inductance and resistance are $L = 0.102mH$ and $R = 2.944\Omega$. By setting pole to 25kHz, the proportional gain k_P and integral gain k_I are obtained as below.

$$k_I = 4619989$$
$$k_P = 160.068 \tag{22}$$

IV. Simulation Results

In order to verify the current controller for the PMEDS, some simulation results are presented. The simulation parameters are shown in Table II.

Because of the limited switching frequency, it is more difficult to control the current when the vibration frequency is high than that is low. The carrier frequency is 50kHz and the V_{dc} is 10V.

Fig. 9 and Fig. 10 are the current command, current and acceleration of the PMEDS with current command 200Hz and 2000Hz, respectively. Fig. 9(a) and Fig. 10(a) operate in unipolar scheme, and Fig. 9(b), Fig. 9(c), Fig. 10(b), and Fig. 10(c) operate in CHB. From Fig. 9, the current and acceleration of Fig. 9(c) are better than those of Fig. 9(a) and Fig. 9(b).

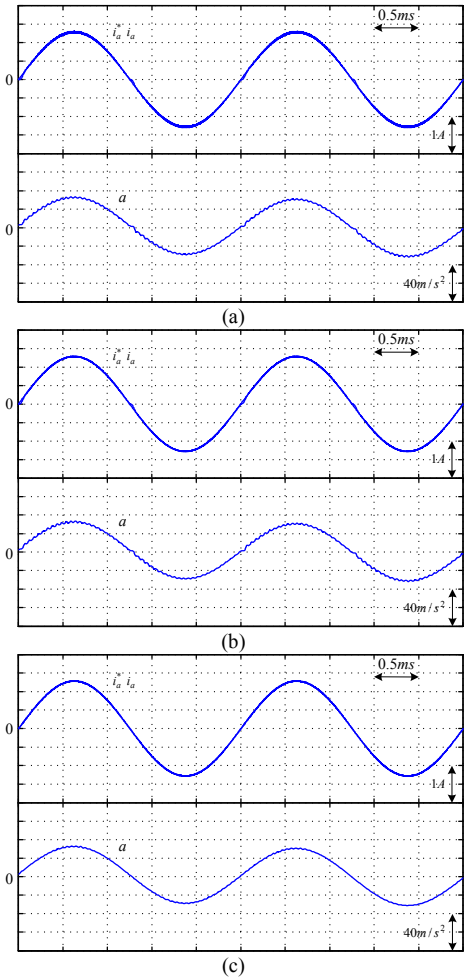

Fig. 9. Simulation results of the PMEDS with current command 200Hz
(a)H-bridge unipolar scheme; (b)CHB;
(c)CHB with dead-time compensator.

The current ripple in Fig. 10(a) is larger than that in Fig. 10(b) and Fig. 10(c), since the ripple frequency of the output voltage in the unipolar scheme is lower than that in the CHB. From Fig. 10(b), the current waveform of CHB without dead-time compensator is not very well, especially near the zero-corssing points. The current of Fig. 10(a) has some high frequency harmonics near the higher resonant frequency 10kHz and contributes the harmonic acceleration . near 10kHz.

From the Fig. 10(c), the current waveform of CHB with dead-time compensator has a better performance. The acceleration also has lower harmonics due to a better current waveform.

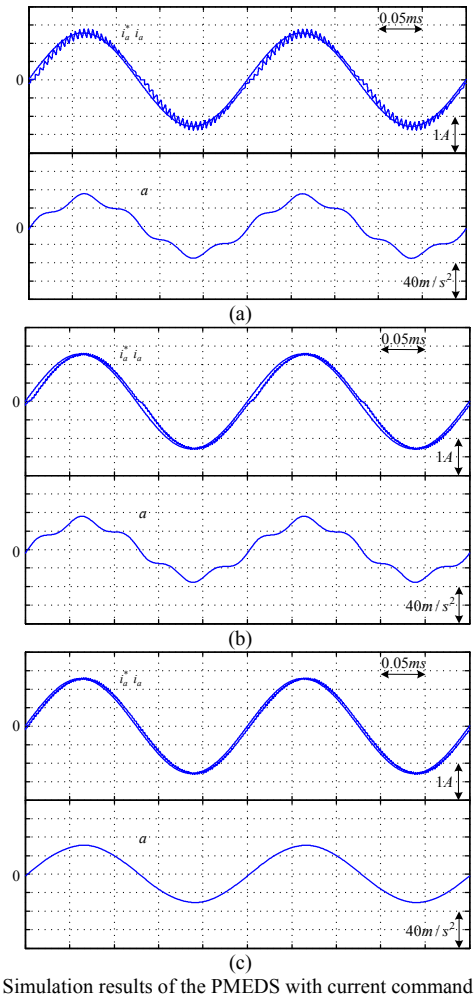

Fig. 10. Simulation results of the PMEDS with current command 2kHz
(a)single H-bridge with unipolar PWM scheme;
(b)CHB without dead-time compensator;
(c)CHB with dead-time compensator.

V. Experimental Results

The direct current control in this paper is implemented by an FPGA-based system using Spartan-3 XC3S200. Fig. 11 is the picture of experimental circuit board. The PMEDS type V406 which is used in this paper is made by Ling Dynamic System Company. Fig. 12 is the experimental results using CHB without dead-time compensator and with it. The vibration frequency is at 2000Hz, the carrier frequency is at 50kHz, and the dead-time is set to $1\mu s$.

As shown in Fig. 12(a), the acceleration contains a component whose frequency is at about 10kHz due to the distorted current. The experimental result of Fig. 12(b) has a better current tracking performance and a lower distorted acceleration.

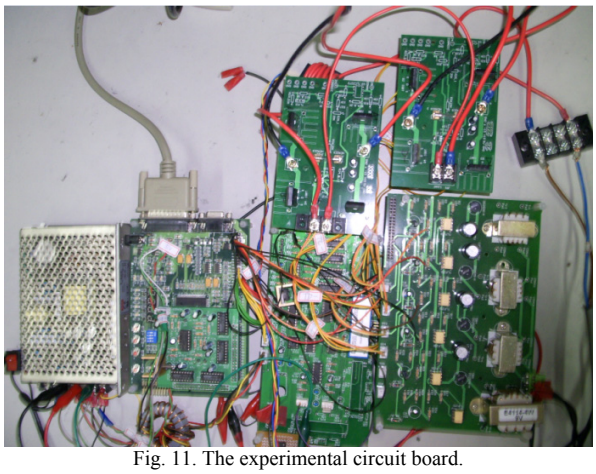

Fig. 11. The experimental circuit board.

Fig. 13 is the spectrum of acceleration of Fig. 12. From Fig. 13(a), the acceleration has the 2kHz and 10kHz components. The 2kHz is the vibration frequency, and the 10kHz is the resonant frequency. By using the dead-time compensator and the CHB, the acceleration harmonics at 10kHz has been reduced.

VI. Conclusions

Traditionally, the vibration control of PMEDS used linear power amplifier which has the disadvantage of heavy weight, huge size, and low efficiency. The PWM switching mode inverter which uses an LC filter may also has these disadvantages. This paper proposed a simply direct current control for the PMEDS. A dead-time compensator and a CHB are used to replace the LC filter which is used to lower the high frequency harmonics. From the simulation and experimental results, the proposed current control has worked well in the CHB.

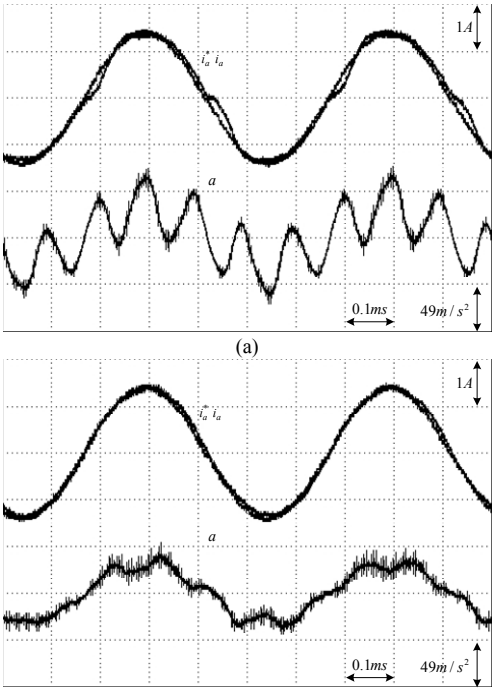

Fig. 12. Experimental results of CHB at 2000Hz
(a)without dead-time compensator;
(b)with dead-time compensator.

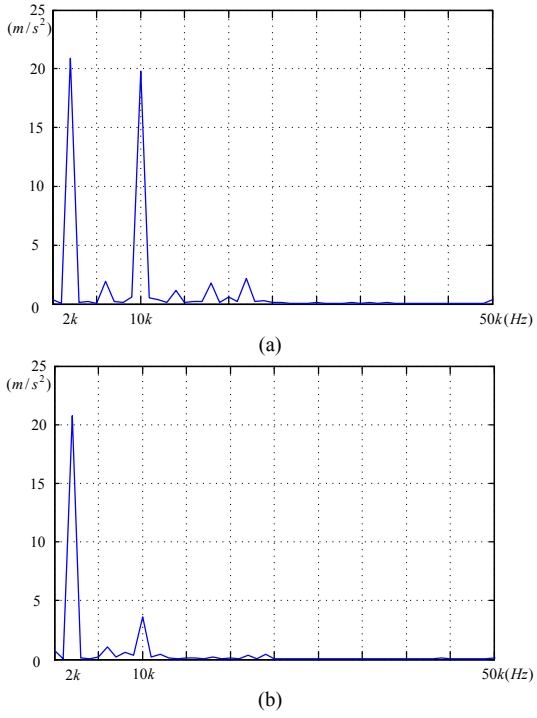

Fig. 13. The spectrum of acceleration of (a)Fig. 12(a); (b)Fig. 12(b).

REFERENCES

[1] C. M. Harris, Shock and Vibration Handbook, New York：McGraw-Hill, 1998.

[2] L. D. Flora and H. A. Grudling, "Time Domain Sinusoidal Acceleration Controller for an Electrodynamic Shaker," *IET Control Theory Appl*., vol. 2, no. 12, pp. 1044–1053, Dec. 2008.

[3] Y. Uchiyama, M. Mukai and M. Fujita "Robust Acceleration Control of Electrodynamic Shaker Using μ-Synthesis," *in Proc. IEEE Conference on Decision and Control* (*CDC*), pp. 6170-6175, 2005.

[4] T. H. Chen and C. M. Liaw, "Vibration Acceleration Control of an Inverter-Fed Electrodynamic Shaker," *IEEE/ASME Trans. on Mechatronics*, vol. 4, no. 1, pp. 60-70, March 1999.

[5] B. J. Kang and C. M. Liaw, "Robust Hysteresis current-controlled PWM Scheme with Fixed Switching Frequency," *IEE Proc.-Electr. Power Appl.,* vol. 148, no. 6, pp. 503-512, Nov. 2001.

[6] C. M. Liaw, W. C. Yu and T. H. Chen, "Random Vibration Test Control of Inverter-Fed Electrodynamic Shaker," *IEEE Trans. on Industrial Electronics*, vol. 49, no. 3, pp. 587-594, June 2002.

[7] J. Han, T. Tang, and X. Wang, "A High-Performance Switching Mode Power Amplifier for Electrodynamic Shaker," *in Proc. IEEE International Conference on Industrial Technology* (*ICIT*), pp. 491-495, 2005.

[8] J. Han, T. Tang, and X. Wang, "Sinusoidal Vibration Test Control of a Switching Mode Power Amplifier-Fed Electrodynamic Shaker," *in Proc. IEEE International Conference on Industrial Electronics and Applications* (*ICIEA*), pp. 1-5, 2006.

[9] L. D. Flora and H. A. Grudling, "Acceleration Control of an Inverter-fed Electrodynamic Shaker," *in Proc. IEEE Power Electronics Specialists Conference* (*PESC*), pp. 2799–2805, Jeju, Korea, June 2006.

[10] L. D. Flora and H. A. Grundling, "Adaptive Acceleration Control of an AC Power Source-Fed Electrodynamic Shaker," *in Proc. IEEE Industry Applications Conference*, pp. 1831-1836, Sept. 2007.

[11] Kwang-Seob Kim, Byung-Ki Kwon and Chang-Ho Choi, "A Novel Control Algorithm of a Three-phase PWM Inverter with Output LC Filter," *in Proc. IEEE Electric Machines & Drives Conference (IEMDC)*, vol. 1, pp. 77-81, May 2007.

[12] O. Kukrer, "Deadbeat control of a three-phase inverter with an output LC filter," IEEE Transactions on Power Electronics, vol. 11, no.1, pp. 16-23, Jan. 1996

[13] M. Kojima, K. Hirabayashi, Y. Kawabata, E. C. Ejiogu and T. Kawabata, "Novel vector control system using deadbeat-controlled PWM inverter with output LC filter," IEEE Transactions on Industry Applications, vol. 40, no. 1, pp. 162-169, Jan. 2004.

[14] T. H. Chen, K. C. Huang and C. M. Liaw, "High-Frequency Switching-Mode Power Amplifier for Shaker Armature Excitation," *IEE Proc.-Electr. Power Appl.,* vol. 144, no. 6, pp. 415-422, Nov. 1997.

[15] I. Colak, E. Kabalci, R. Bayindir and S. Sagiroglu, "The Design and Analysis of a 5-Level Cascaded Voltage Source Inverter with Low THD," POWERENG Conf., pp 575-580, Lisbon, Mar. 2009.

[16] A. A. Sneineh, M. Y. Wang, and K. Tian, "A Hybrid Capacitor-Clamp Cascade Multilevel Converter," *in Proc. IEEE IECON*, pp. 2031-2036, Paris, Nov. 2006.

[17] V. K. Chinnaiyan, J. Jerome, J. Karpagam, and T. Suresh, "Control techniques for multilevel voltage source inverters," *in Proc. IPEC*, pp. 1023-1028, Singapore, Dec. 2007.

[18] P. Panagis, F. Stergiopoulos, P. Marabeas, and S. Manias, "Comparison of state of the art multilevel inverters," *in Proc. IEEE PESC*, pp 4296-4301, Rhodes, Jun. 2008.

[19] P. Karuppanan, K. K. Mahapatra, "FPGA based cascaded multilevel pulse width modulation for single phase inverter" *in Proc. Environment and Electrical Engineering International Conf*., pp. 273-276, Prague, May 2010.

[20] D.W Kang, B.K. Lee, J.H. Jeon, T.J. Kim and D.S. Hyun, "A symmetric carrier technique of CRPWM for voltage balance method of flying-capacitor multilevel inverter," *IEEE Transactions on Industrial Electronics*, vol .52,no. 3, pp. 879-888, Jun. 2005